Role of dynamic pairing correlations in fission dynamics

R. Bernard,[1,2] S. A. Giuliani,[3] and L. M. Robledo[4,5,*]

[1]*Centre de Mathématiques et de Leurs Applications, CNRS, ENS Paris-Saclay, Université Paris-Saclay, 94235 Cachan Cedex, France*

[2]*CEA, DAM, Île-de-France, 91297 Arpajon, France*

[3]*NSCL/FRIB Laboratory, Michigan State University, East Lansing, Michigan 48824, USA*

[4]*Center for Computational Simulation, Universidad Politécnica de Madrid, Campus de Montegancedo, Boadilla del Monte, 28660 Madrid, Spain*

[5]*Departamento de Física Teórica, Universidad Autónoma de Madrid, 28049 Madrid, Spain*

(Received 14 March 2019; published 3 June 2019)

We study the role of dynamic pairing correlations in fission dynamics by considering intrinsic Hartree-Fock-Bogoliubov wave functions that are obtained by minimizing the particle number projected energy. For the restricted variational space, the set of self-consistent wave functions with different values of proton and neutron number particle fluctuations are considered. The particle number projected energy is used to define the potential energy surface for fission whereas collective inertias are computed within the traditional formulas for the intrinsic states. The results show that the effect of the restricted variation after particle number projection in the potential energy surface is small while collective inertias substantially decrease. On the other hand, we show that this quenching is strongly mitigated when Coulomb antipairing is considered and therefore the final outcome of the complete calculation is close to the plain mean field result without Coulomb antipairing. In the light of these beyond-mean-field calculations, the validity of traditional fission calculations is discussed.

DOI: 10.1103/PhysRevC.99.064301

I. INTRODUCTION

Undoubtedly, pairing correlations represent a key ingredient in the description of the dynamics of the fission phenomenon experienced by heavy atomic nuclei [1,2]. For instance, the amount of pairing correlations has a strong impact on quantities such as spontaneous fission lifetimes [3–13], the shape of the barriers separating the ground state from scission [14–20], and fission fragments distributions [21–24]. At the mean-field level, pairing is traditionally described using the Hartree-Fock-Bogoliubov (HFB) theory, which is a reasonable approximate scheme when pairing correlations are strong [25]. In nuclear physics, however, the pairing strength is not strong enough and, as a consequence, many mean field configurations show little or no pairing correlations at all [26,27]. In this case the mean-field description of the nucleus breaks down, and the inclusion of dynamic pairing correlations stemming from beyond-mean-field effects becomes necessary. The evolution of the nucleus through the different shapes involved in fission affects the level density around the Fermi energy, with a large impact on pairing correlations. This effect is reflected by the intricate behavior shown along the fission path, including many regions of very weak static pairing, which points out the possible crucial role of dynamic pairing correlations in the studies of fission.

In order to account for such effects, beyond-mean field calculations involving the restoration of the particle number of the nuclear wave function are required. Unfortunately the computational cost of beyond-mean-field calculations has limited so far their application to fission studies, keeping the impact of dynamic pairing correlations unexplored. Moreover, to properly address the role of dynamic pairing correlation one should account for all those effects that may mitigate the effective pairing strength and that are usually neglected for the sake of computational time, for instance Coulomb antiparing [28], which is the name given to the destructive effect of the repulsive Coulomb interaction in the proton's pairing correlations. If proton and neutron pairing strengths are independently adjusted to experimental data in the region of interest [29], Coulomb antipairing is taken into account in an effective way by the fitted pairing strengths. Conversely, in forces like Gogny [30] the neutron pairing strength is fitted to experimental data (for instance in the tin isotopic chain) and the proton pairing strength comes from isospin invariance. In those cases, Coulomb antipairing must be explicitly taken into account to avoid the self-energy problem and the breaking of the Pauli principle in particle number projected calculations. The Coulomb antipairing effect can reduce the proton's pairing gap by 20–30% [31,32], with a strong impact on observables such as moments of inertia [28,33], but its effect is usually neglected due to the enormous computational cost associated with the evaluation of Coulomb's pairing field [28].

In the light of this discussion, it is possible to conclude that the inclusion of dynamic pairing will have a twofold effect: On the one hand, collective inertias driving fission dynamics, with their inverse dependence on the square of

*lm.robledo.physics@gmail.com

the pairing gap [1,12,34,35], are expected to increase when the Coulomb antipairing effect is considered, increasing the collective action and leading to longer fission lifetimes $t_{\rm SF}$. On the other hand, dynamic pairing correlations are expected to increase the pairing gap reducing thereby the collective inertias. The outcome of these competing effects is uncertain and it is the purpose of this paper to clarify this situation and establish a step forward in the study of beyond-mean-field effects in fission calculations.

In previous studies, angular momentum projection [36] has been used to compute fission barrier heights. However, the results are almost indistinguishable from the ones obtained with rotational correction [2,37]. Parity projection has also been considered in the reflection asymmetric section of the fission path [16,38], with little or no impact at all. Finally, the impact of particle number projection on fission barrier heights has been considered in [16]. A change of at most ± 0.5 MeV is obtained in all the cases.

In this paper we are considering the contribution to dynamic pairing correlation coming from a restricted variation after projection for particle number projection. The evolution of the pairing properties of the nucleus as it evolves towards fission will be studied as a function of the axial quadrupole moment $q = \langle Q_{20} \rangle$. We will analyze the impact of dynamic pairing correlations on the potential energy surface, computed with the particle number projected wave function $|\Psi^N(q)\rangle = \hat{P}^N|\varphi(q)\rangle$, and on the collective inertia computed with the intrinsic state $|\varphi(q)\rangle$.

II. METHODOLOGY

Dynamic pairing correlations require a beyond-mean-field framework involving the restoration of the particle quantum number of the nuclear wave function. In order to gain more correlations, the intrinsic mean field wave function has to be determined by minimizing the projected energy in the so- called variation after projection (VAP) method. In this paper we use the restricted variation after projection (RVAP) [39] particle number projection (PNP) method [40]. The RVAP-PNP method has been shown to be superior to other alternatives like the Lipkin-Nogami method commonly used in the literature [39]. In the RVAP-PNP method the variational subspace is formed by projecting onto good particle number (protons and neutrons separately) intrinsic wave functions obtained from a HFB calculation constraining the particle number fluctuation for protons and neutrons $|\Phi(\langle \Delta Z^2 \rangle_\pi, \langle \Delta N^2 \rangle_\nu)\rangle$.[1] Henceforth, we will use new variables $f_\nu = \langle \Delta N^2 \rangle$ and $f_\pi = \langle \Delta Z^2 \rangle$ to alleviate notation. The RVAP intrinsic state $|\Phi(f_\pi, f_\nu)\rangle$ corresponds to the minimum of the projected energy

$$E^{Z,N}(f_\pi, f_\nu) = \frac{\langle \Phi(f_\pi, f_\nu)|\hat{H}P^Z P^N|\Phi(f_\pi, f_\nu)\rangle}{\langle \Phi(f_\pi, f_\nu)|\Phi(f_\pi, f_\nu)\rangle}, \quad (1)$$

[1]The constraint on $\langle \Delta N^2 \rangle$ involves the two-body operator $\Delta\hat{N}^2$. The implementation of this constraint is straightforward when using the gradient method to solve the HFB equation [41].

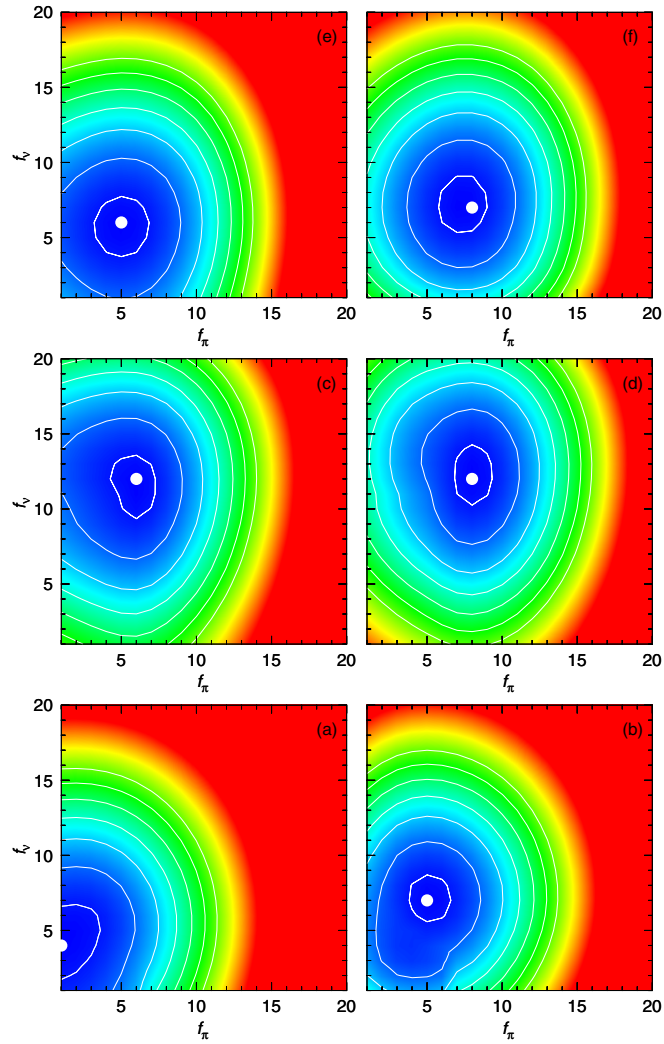

FIG. 1. In the left (right) panels contour plots of the HFB (PNP) energy as a function of $f_\nu = \langle \Delta N^2 \rangle$ and $f_\pi = \langle \Delta Z^2 \rangle$ are given for three different quadrupole moments, namely, $Q_2 = 14$b (ground state) [panels (a) and (b)], $Q_2 = 28$b (first fission barrier) [panels (c) and (d)], and $Q_2 = 42$b (fission isomer) [panels (e) and (f)]. The results are obtained with the Gogny D1M force for the nucleus ^{240}Pu. The minima are marked by a dot and the color range spans 5 MeV.

as a function of the f_π and f_ν variables. The minimum of the two-dimensional function $E^{Z,N}(f_\pi, f_\nu)$ is determined by a simple gradient method in two dimensions. The potential energy surface for fission is obtained by introducing an additional constraint on the quadrupole moment Q_{20} of the axially symmetric intrinsic state and is given by the projected energy of the RVAP for each Q_{20} value. We could also introduce easily additional constrains like the octupole moment or the necking operator to form multidimensional potential energy surfaces (PESs) which are so popular in fission studies, but this is not the purpose of the present work. An example of both the HFB and PNP potential energy surfaces obtained as a function of f_ν and f_π is given in Fig. 1, where those energies, computed with the Gogny D1M parametrization [42], are plotted for the nucleus ^{240}Pu and three different

values of the quadrupole moment (see caption for details). The chosen quadrupole moments correspond to the ground state, first fission barrier, and fission isomer. Both the HFB and PNP energies show a parabolic behavior as a function of (f_π, f_ν) that is slightly distorted in both cases. In the figure, it is clearly observed how the minimum of the PNP energy is shifted to higher f_ν and f_π values as compared to the HFB ones. This is in agreement with the expectation that the RVAP method provides intrinsic states with more pairing correlations than those intrinsic states obtained by the HFB method. This has important consequences for fission dynamics, as the collective inertia strongly depends upon the amount of pairing correlations.

The other quantity required to study the dynamics of spontaneous fission is the collective inertia associated with the collective variables used to drive the nucleus from its ground state to fission. The collective inertia plays a crucial role in several fission observables, such as the spontaneous fission lifetimes $t_{\rm SF}$ obtained within the Wenzel-Kramers-Brillouin (WKB) formula and the fission fragments distributions obtained in both time dependent frameworks [21,43] and stochastic Langevin approaches [22,24]. For instance, the $t_{\rm SF}$ has an exponential dependence on the collective inertia than can amount to changes of several orders of magnitude in this quantity [10–12]. As mentioned before, the magnitude of the collective inertia depends on the amount of pairing correlations in a way that can be quantified as an inverse dependence on the square of the pairing gap. This dependence on the amount of pairing correlations implies that the larger the pairing correlations are, the smaller the collective inertia (and therefore $t_{\rm SF}$) is. Therefore, we expect a strong dependence of the collective inertia on the combined action of both the Coulomb antipairing effect and the PNP.

There are two types of collective inertias: the one coming from adiabatic time dependent Hartree-Fock-Bogoliubov (ATDHFB) theory and the one coming for the Gaussian overlap approximation (GOA) to the generator coordinate method (GCM) [2]. Unfortunately, so far none of these schemes has been generalized to the case of non-HFB states like the PNP ones considered in this paper. In these respect, the GCM-GOA framework is more promising since its formalism is not intimately rooted to the HFB method. However, the perturbative cranking approximation (where the linear response matrix is approximated by its diagonal both in the expressions of the inertia and in the definition of the collective momentum [44]), required to alleviate the computational cost of the evaluation of the collective inertias, is not easy to implement in the PNP case. Therefore we take a pragmatic approach and use for the PNP case the perturbative cranking inertias computed with the intrinsic state $|\Phi\rangle$ obtained in the RVAP. Work to obtain a sound and easy way to compute the inertia for PNP wave functions is under way and will be reported elsewhere.

To avoid the appearance of divergences in the calculation of the PNP energy with the Gogny force, we computed the exchange, direct, and pairing channels for each of the terms of the interaction [40]. The required Hamiltonian and norm overlap between the HFB state $|\Phi\rangle$ and the one rotated in gauge space, $e^{i\Phi_p\hat{Z}}e^{i\Phi_n\hat{N}}|\Phi\rangle$, are computed using the methodology of

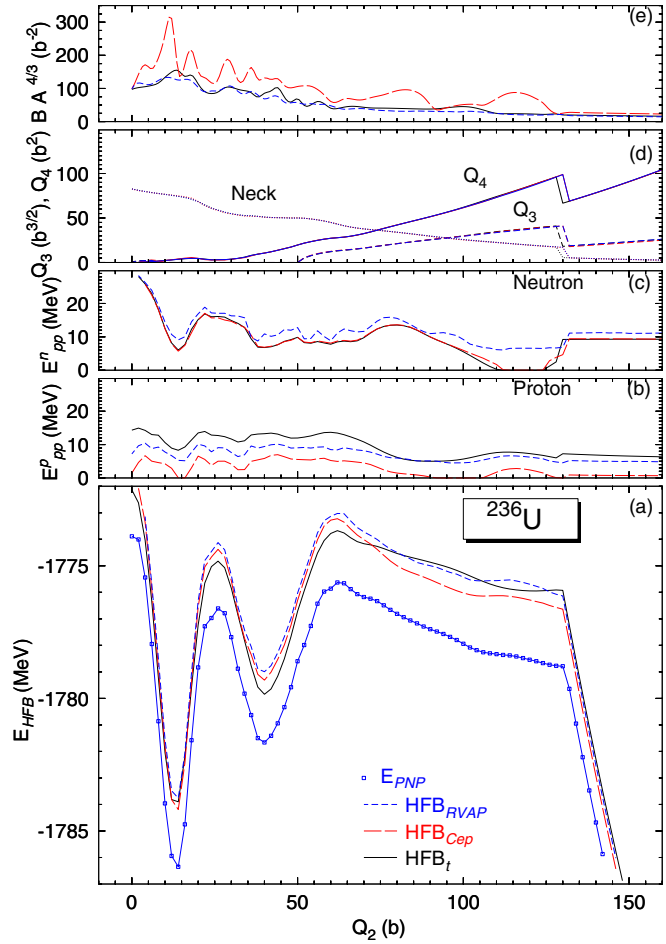

FIG. 2. In panel (a) the potential energies obtained in the different approaches discussed in the text are plotted as as function of the quadrupole moment of the intrinsic state. The color code and the labels are described in the main text. In panels (b) and (c) the particle-particle correlation energy $\frac{1}{2}\mathrm{Tr}\Delta_\tau\kappa_\tau$ for protons and neutrons, respectively, is given. The octupole, hexadecapole and neck parameters are given in panel (d). Finally, in panel (e) the ATDHFB quadrupole collective inertia computed in the perturbative approximation is given.

the generalized Wick theorem as developed in [45,46]. For the density dependent part of the interaction we use the so-called PNP projected density prescription that is commonly used for particle number projection [40,47] (be aware, however, of the fundamental difficulties encountered when using the projected density prescriptions in the context of spatial symmetries restoration [48]).

III. RESULTS

We have considered three nuclei as prototypical examples illustrating the issues discussed in the previous section. The first nucleus studied is the light actinide ^{236}U, characterized by a double humped potential energy surface (PES) with high and wide barriers. Reflection symmetry is broken right after the fission isomer and therefore asymmetric fragment mass distribution is expected for this nucleus. In Fig. 2 we show

TABLE I. On the left-hand side, spontaneous fission half-lives (in seconds) computed with two different sets of collective inertias (ATDHFB and GCM) and for the four different sets of calculations for the nuclei considered. On the right-hand side, the values of the fission barrier heights B_I, B_{II}, and fission isomer excitation energy E_{II} (in MeV) are also given.

		t_{SF}				
		ATDHFB (s)	GCM (s)	B_I (MeV)	E_{II} (MeV)	B_{II} (MeV)
^{236}U	HFB_t	3.0×10^{43}	2.4×10^{32}	9.07	4.05	10.22
	HFB_{Cep}	3.1×10^{63}	1.2×10^{46}	9.82	4.88	10.97
	HFB_{RVAP}	8.3×10^{41}	1.1×10^{32}	9.64	4.77	10.74
	PNP	1.0×10^{42}	1.4×10^{32}	9.74	4.69	10.72
^{240}Pu	HFB_t	7.4×10^{38}	7.5×10^{29}	10.23	4.39	10.20
	HFB_{Cep}	2.0×10^{54}	2.4×10^{39}	10.91	4.94	10.75
	HFB_{RVAP}	3.0×10^{37}	9.5×10^{28}	10.74	4.74	10.57
	PNP	2.8×10^{37}	1.2×10^{29}	10.83	4.79	10.63
^{252}Cf	HFB_t	2.3×10^{22}	1.7×10^{18}	11.18	3.71	7.77
	HFB_{Cep}	7.6×10^{24}	2.9×10^{18}	11.60	3.45	6.86
	HFB_{RVAP}	7.8×10^{19}	2.5×10^{15}	11.19	3.40	7.09
	PNP	1.9×10^{21}	6.2×10^{16}	11.22	3.71	7.49

the most relevant quantities for a theoretical understanding of fission. In panel 2(a) potential energy surfaces (to be discussed below) are shown as a function of the quadrupole moment. The corresponding particle-particle correlation energies $\frac{1}{2}\mathrm{Tr}(\Delta_\tau \kappa_\tau)$ (with $\tau = p, n$) are shown in panels 2(b) and 2(c). In panel 2(d) the self-consistent octupole and hexadecapole moments are also shown along with the neck parameter given by the mean value of the neck operator $Q_N = \exp[-(z - z_0)^2/a_0^2]$ with $z_0 = 0$ and $a_0 = 1.0$ fm. Finally, in panel 2(e) the collective inertia computed in the traditional perturbative ATDHFB scheme is displayed.

Panel 2(a) shows the potential energy surfaces for four different calculations. The black solid line (HFB_t) corresponds to the traditional HFB calculation where Coulomb exchange is evaluated in the Slater approximation and Coulomb and spin-orbit antipairing are neglected. The dashed red line (HFB_{Cep}) corresponds to a HFB calculation where both Coulomb exchange and antiparing are fully considered. Comparing the predicted isomer energies (E_{II}) and inner (B_I) and outer (B_{II}) fission barrier heights (see Table I) we notice that HFB_{Cep} predicts values that are 0.75–0.83 MeV larger. This increase is an expected behavior when pairing correlations get reduced [11,16]. Also, more pronounced structures are observed in HFB_{Cep}, particularly at large quadrupole deformations, which can be traced back to the reduced pairing correlations [49] associated with the presence of Coulomb antipairing. These changes in the potential energy surface are partially washed out in the HFB calculation obtained with intrinsic RVAP states (HFB_{RVAP}, blue dashed line). The HFB_{RVAP} barriers heights and isomer excitation energy are 0.52–0.55 larger than the HFB_t, and the potential energy surfaces at large deformations are also similar. This result suggests that pairing correlations induced by the RVAP partially cancel out the effect of the Coulomb antipairing quenching (see below). Finally, the blue full curve with symbols corresponds to the RVAP projected energy (E_{PNP}). This energy is around two MeV deeper than the intrinsic energies, the fission parameters being 0.50–0.64 MeV larger than the HFB_t results.

In order to better understand the impact of dynamic correlations on fission, it is worthwhile to analyze the changes in the other quantities depicted in Fig. 2. Proton particle-particle correlation energies are shown in panel 2(b) for the HFB_t, HFB_{Cep}, and HFB_{RVAP} intrinsic states (this quantity is meaningless in the PNP case). Coulomb antipairing quenches the particle-particle proton correlation energy, but the quenching is softened by the effect of the PNP-RVAP, the latter results being closer to the HFB_t ones. In the neutron case, shown in panel 2(c), no significant differences are observed between the HFB_t and HFB_{Cep} cases as expected. The effect of PNP-RVAP is to increase neutron pairing correlations, bringing the particle-particle correlation energy of the intrinsic state above the other two curves. The quadrupole, octupole, and necking shape parameters are shown in panel 2(d). For each of the three parameters, the results obtained with the three different types of intrinsic states lie each on top of the other. The impact on the deformation parameters of using different types of treatments for the pairing correlation is negligible. Finally, in panel 2(e) the ATDHFB perturbative collective inertias for the three intrinsic states are shown. Compared to the HFB_t reference calculation, the HFB_{Cep} inertia is larger as a consequence of the quenched pairing. Overall, the HFB_{Cep} inertia is around two times larger than the HFB_t one. It also shows more pronounced structures in the form of high peaks. On the other hand, the increase of pairing correlations associated with PNP-RVAP brings the HFB_{RVAP} intrinsic inertia back to the range of the HFB_t curve. It is worth mentioning that the HFB_{RVAP} inertia looks a bit smoother than the HFB_t one. From this comparison we conclude that the HFB_t inertia (i.e., without Coulomb exchange, and, what is more important, without Coulomb antipairing) represents a good approximation, in the case of the Gogny force, to the inertia obtained from the PNP-RVAP intrinsic states. It is worth mentioning that this cancellation is typical of the Gogny forces and is not expected in calculations where the strength of the pairing interaction is fitted separately for protons and neutrons to experimental data [50]. In this case, the effect of Coulomb antipairing is taken into account by the fitted pairing strength, and therefore a reduction of a factor of 2 in the inertias has to be expected in the PNP-RVAP case. This reduction could be mitigated if the fitting of the pairing strength is carried out at the PNP-RVAP level.

Finally, we have computed the spontaneous fission half-life t_{SF} using the traditional WKB formula (see Refs. [2,11] for details and applications) with an E_0 parameter of 1 MeV. The results for the HFB_t and HFB_{Cep} cases are computed with the corresponding PES and collective inertias, whereas the PNP-RVAP is computed with the PNP PES but using the collective inertia of the HFB_{RVAP} intrinsic state. The results are summarized in Table I along with the values of E_{II}, B_I, and B_{II} discussed above. The effect of Coulomb antipairing on the inertia is to increase t_{SF} by 20 (14) orders of magnitude in the ATDHFB (GCM) cases, but this huge impact is canceled out

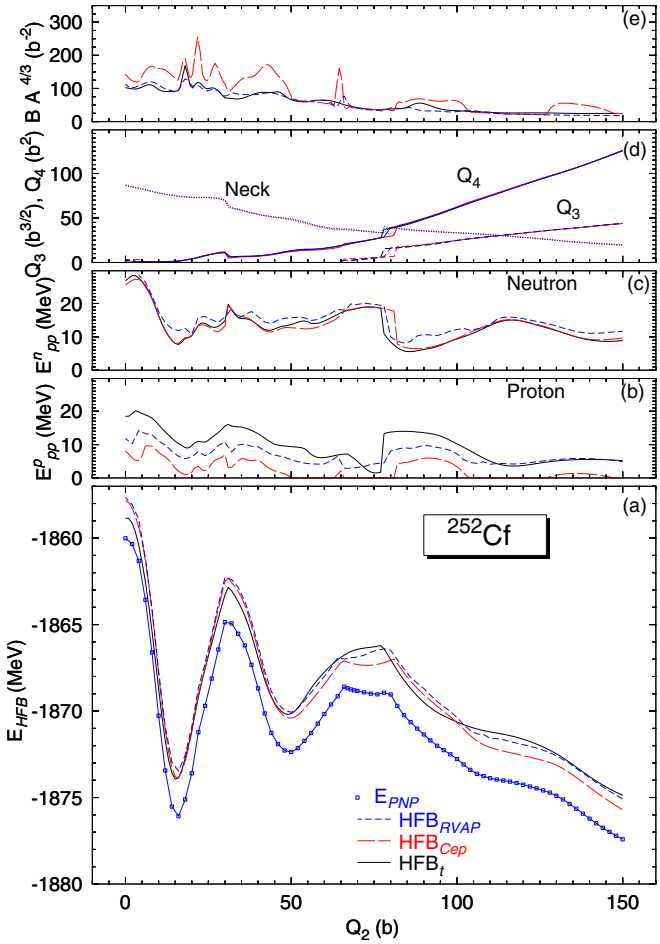

FIG. 3. Same as Fig. 2 but for the nucleus ^{252}Cf.

by the dynamic pairing effect associated with RVAP-PNP. The final RVAP-PNP t_{SF} values are very close to the HFB$_t$ ones. It is important to emphasize that the RVAP-PNP t_{SF} values are lower than the HFB$_t$ ones in spite of the larger fission barrier heights. This is due to the smaller values of the inertias in the projected case.

The results obtained for the nucleus ^{240}Pu look qualitatively the same as those obtained for ^{236}U, the small differences observed being mostly due to shell effects associated with the different proton and neutron numbers. The values of E_{II}, B_I, and B_{II} are given in Table I. The most notorious difference is in the larger values of B_I, which are around 1 MeV higher than in the ^{236}U case. The impact of Coulomb antipairing on t_{SF} is 16 (10) orders of magnitude for the ATDHFB (GCM) inertias and, as in the uranium case, the inclusion of dynamical pairing correlations reduces substantially t_{SF} and brings it closer to the traditional HFB$_t$ value. As in the previous case, we conclude that dynamic pairing compensates for the Coulomb antipairing effect, and the t_{SF} values obtained in the traditional HFB approach are very similar to the ones obtained in the RVAP-PNP context.

We have also carried out calculations for the heavier ^{252}Cf isotope. The potential energy surfaces, particle particle energy correlations, deformation parameters and ATDHFB collective inertias are shown in Fig. 3. In all the cases, the PESs show a rather high inner barrier (see Table I for the values of the different parameters). The reflection symmetric fission isomer lies at around 3.7 MeV excitation energy, whereas the slightly reflection asymmetric outer barrier is around 7 MeV high. In this particular nucleus the impact of the different theoretical schemes used in the calculation of the outer barrier is stronger, with changes in its height of more than 1 MeV. It turns out that in the region of the outer barrier the HFB$_t$ PES is very flat with several coexisting minima, but one of them is clearly favored when Coulomb antipairing is considered. The particle-particle correlation energy for protons looks similar to the one of ^{236}U for the HFB$_{Cep}$ and HFB$_{RVAP}$ cases but differs significantly from the HFB$_t$ value around the outer barrier region. The reason for this behavior is the same reason that explains the discrepancies in the PESs in that region. The E_{pp} for neutrons follows the same pattern as in the uranium case and only small differences are noticed in the outer barrier region. The same observation is valid for the deformation parameters of panel 3(d). The behavior of the ATDHFB inertia in panel 2(e) is qualitatively similar to the one of ^{236}U.

Concerning t_{SF}, we observe longer values when Coulomb antipairing is considered, but the difference amounts to 2 (0) orders of magnitude in the ATDHFB (GCM) case. This is in strong contrast with the ^{236}U and ^{240}Pu cases. A possible explanation is the reduction of the outer barrier height of more than 1 MeV seen in this particular case. Considering dynamical pairing lowers t_{SF} by 5 (3) orders of magnitude in the ATDHFB (GCM) cases as compared to the HFB$_{Cep}$ result. The net effect of these opposite trends is to yield final values for the RVAP-PNP calculation which are, again, pretty close to the HFB$_t$ ones.

IV. CONCLUSIONS

In this paper we studied the impact of dynamical pairing correlations in the theoretical estimation of fission properties. We found that particle number projection in the restricted variation after projection framework (using $\langle \Delta N^2 \rangle$ for protons and neutrons as variational parameters) has a profound impact on some of the quantities related to fission, such as spontaneous fission half-lives. The parameters defining the potential energy surface, like the fission barrier heights and fission isomer location, are little affected by particle number projection in the three examples analyzed. On the other hand, the increase in pairing correlations due to particle number restoration leads to a quenching of the collective inertia by a factor of the order of 2. The consequences for the spontaneous fission half-life depend on the nucleus, but it is quantified to be large and can reach a reduction of 20 orders of magnitude. This reduction is compensated by the Coulomb antipairing effect, which is often neglected in mean field calculations but is required in particle number projection to avoid the self-energy and self-pairing problems. The reduction of pairing correlations associated with Coulomb antipairing increases the collective inertias by a factor of around 2 in the examples considered and can increase the calculated t_{SF} up to 20 orders of magnitude. On the other hand, the consequences of an exact treatment of the Coulomb exchange potential in the potential energy surface are relatively small and have a relatively less important

impact on t_{SF}. The two opposite effects, Coulomb antiparing and dynamical pairing correlations, tend to suppress each other, and the final outcome turns out to be similar to the results obtained omitting both of them. This result is relevant for calculations with nuclear forces (Gogny among them), where the nuclear pairing interaction is isospin invariant and Coulomb antipairing has to be considered. The effect of dynamical pairing correlations alone is relevant for other interactions where the pairing strength for protons and neutrons used at the mean field level is fitted to experimental data.

For future work, the evaluation of the collective inertias with particle number projected wave functions is the next step to consider. Also, the consequences of particle number projection on induced fission half-lives and properties of the fission fragments could be an interesting subject of research.

ACKNOWLEDGMENTS

S.A.G. acknowledges support from the U.S. Department of Energy under Grant No. DOE-DE-NA0003885 (NNSA, the Stewardship Science Academic Alliances program). The work of L.M.R. has been supported in part by Spanish Grants No. FIS2015-63770 MINECO and No. FPA2015-65929 MINECO.

[1] L. Moretto and R. Babinet, Phys. Lett. B **49**, 147 (1974).
[2] N. Schunck and L. M. Robledo, Rep. Prog. Phys. **79**, 116301 (2016).
[3] M. Urin and D. Zaretsky, Nucl. Phys. **75**, 101 (1966).
[4] A. Staszczak, A. Baran, K. Pomorski, and K. Böning, Phys. Lett. B **161**, 227 (1985).
[5] Y. A. Lazarev, Phys. Scr. **35**, 255 (1987).
[6] A. Staszczak, S. Piłat, and K. Pomorski, Nucl. Phys. A **504**, 589 (1989).
[7] Z. Łojewski and A. Staszczak, Nucl. Phys. A **657**, 134 (1999).
[8] K. Pomorski, Int. J. Mod. Phys. E **16**, 237 (2007).
[9] M. Mirea and R. C. Bobulescu, J. Phys. G: Nucl. Part. Phys. **37**, 055106 (2010).
[10] S. A. Giuliani and L. M. Robledo, Phys. Rev. C **88**, 054325 (2013).
[11] R. R. Rodríguez-Guzmán and L. M. Robledo, Phys. Rev. C **89**, 054310 (2014).
[12] S. A. Giuliani, L. M. Robledo, and R. R. Rodríguez-Guzmán, Phys. Rev. C **90**, 054311 (2014).
[13] J. Zhao, B.-N. Lu, T. Nikšić, D. Vretenar, and S.-G. Zhou, Phys. Rev. C **93**, 044315 (2016).
[14] W. Stepień and Z. Szymański, Phys. Lett. B **26**, 181 (1968).
[15] K. Rutz, M. Bender, P.-G. Reinhard, and J. A. Maruhn, Phys. Lett. B **468**, 1 (1999).
[16] M. Samyn, S. Goriely, and J. M. Pearson, Phys. Rev. C **72**, 044316 (2005).
[17] N. Schunck, D. Duke, H. Carr, and A. Knoll, Phys. Rev. C **90**, 054305 (2014).
[18] H. Abusara, A. V. Afanasjev, and P. Ring, Phys. Rev. C **82**, 044303 (2010).
[19] S. Karatzikos, A. Afanasjev, G. Lalazissis, and P. Ring, Phys. Lett. B **689**, 72 (2010).
[20] J. Sadhukhan, J. Dobaczewski, W. Nazarewicz, J. A. Sheikh, and A. Baran, Phys. Rev. C **90**, 061304(R) (2014).
[21] H. Goutte, J. F. Berger, P. Casoli, and D. Gogny, Phys. Rev. C **71**, 024316 (2005).
[22] J. Sadhukhan, W. Nazarewicz, and N. Schunck, Phys. Rev. C **93**, 011304(R) (2016).
[23] H. Tao, J. Zhao, Z. P. Li, T. Nikšić, and D. Vretenar, Phys. Rev. C **96**, 024319 (2017).
[24] Z. Matheson, S. A. Giuliani, W. Nazarewicz, J. Sadhukhan, and N. Schunck, Phys. Rev. C **99**, 041304(R) (2019).
[25] P. Ring and P. Schuck, in *The Nuclear Many-Body Problem*, 1st ed. (Springer, Berlin, 1980), pp. 1–718.
[26] D. J. Dean and M. Hjorth-Jensen, Rev. Mod. Phys. **75**, 607 (2003).
[27] D. Brink and R. Broglia, *Nuclear Superfluidity: Pairing in Finite Systems*, Cambridge Monographs on Particle Physics, Nuclear Physics and Cosmology (Cambridge University Press, Cambridge, 2005).
[28] M. Anguiano, J. L. Egido, and L. M. Robledo, Nucl. Phys. A **683**, 227 (2001).
[29] G. F. Bertsch, C. A. Bertulani, W. Nazarewicz, N. Schunck, and M. V. Stoitsov, Phys. Rev. C **79**, 034306 (2009).
[30] J. Dechargé and D. Gogny, Phys. Rev. C **21**, 1568 (1980).
[31] T. Lesinski, T. Duguet, K. Bennaceur, and J. Meyer, Eur. Phys. J. A **40**, 121 (2009).
[32] H. Nakada and M. Yamagami, Phys. Rev. C **83**, 031302(R) (2011).
[33] A. V. Afanasjev, Phys. Scr. **89**, 054001 (2014).
[34] M. Brack, J. Damgaard, A. S. Jensen, H. C. Pauli, V. M. Strutinsky, and C. Y. Wong, Rev. Mod. Phys. **44**, 320 (1972).
[35] G. F. Bertsch and H. Flocard, Phys. Rev. C **43**, 2200 (1991).
[36] M. Bender, P.-H. Heenen, and P. Bonche, Phys. Rev. C **70**, 054304 (2004).
[37] R. R. Rodríguez-Guzmán, J. L. Egido, and L. M. Robledo, Phys. Rev. C **62**, 054319 (2000).
[38] T. V. Nhan Hao, P. Quentin, and L. Bonneau, Phys. Rev. C **86**, 064307 (2012).
[39] T. R. Rodríguez, J. L. Egido, and L. M. Robledo, Phys. Rev. C **72**, 064303 (2005).
[40] M. Anguiano, J. L. Egido, and L. M. Robledo, Nucl. Phys. A **696**, 467 (2001).
[41] L. M. Robledo and G. F. Bertsch, Phys. Rev. C **84**, 014312 (2011).
[42] S. Goriely, S. Hilaire, M. Girod, and S. Péru, Phys. Rev. Lett. **102**, 242501 (2009).
[43] D. Regnier, N. Dubray, N. Schunck, and M. Verrière, Phys. Rev. C **93**, 054611 (2016).
[44] S. A. Giuliani and L. M. Robledo, Phys. Lett. B **787**, 134 (2018).
[45] L. M. Robledo, Phys. Rev. C **79**, 021302(R) (2009).
[46] G. F. Bertsch and L. M. Robledo, Phys. Rev. Lett. **108**, 042505 (2012).
[47] L. M. Robledo, Int. J. Mod. Phys. E **16**, 337 (2007).
[48] L. M. Robledo, J. Phys. G: Nucl. Part. Phys. **37**, 064020 (2010).
[49] G. F. Bertsch, W. Younes, and L. M. Robledo, Phys. Rev. C **97**, 064619 (2018).
[50] A. Baran, M. Kowal, P.-G. Reinhard, L. M. Robledo, A. Staszczak, and M. Warda, Nucl. Phys. A **944**, 442 (2015).